ChemPubSoc Europe

DOI: 10.1002/chem.201801671

CHEMISTRY
A European Journal
Full Paper

Magnetic Resonance Imaging

Hydrazo-CEST: Hydrazone-Dependent Chemical Exchange Saturation Transfer Magnetic Resonance Imaging Contrast Agents

Trina Dang,[a] Mojmír Suchy,[a, b] Yen J. Truong,[a] Wendy Oakden,[c] Wilfred W. Lam,[c] Caitlin Lazurko,[a] Glenn Facey,[a] Greg J. Stanisz,[c, d, e] and Adam J. Shuhendler*[a, b]

Abstract: The rapid formation of hydrazones under physiological conditions was exploited for the detection of aldehydes through chemical exchange saturation transfer magnetic resonance imaging (CEST-MRI). A metal-free, diamagnetic contrast agent derived from N-amino anthranilic acid was introduced, which selectively "turned-on" upon hydrazone formation through an effect termed Hydrazo-CEST. While the hydrazine form of the probe produced no CEST-MRI signal enhancement, the formation of the aryl hydrazone resulted in $>20\%$ intensity decrease in the bulk water signal through the CEST effect, as measured by 300 MHz ^{1}H NMR, 3 T and 7 T MRI. Both the electronic contributions of the N-amino anthranilate and the aldehyde binding partner were shown to directly impact the exchange rate of the proton on the ring-proximal nitrogen, and thus the imaging signal. Additionally, the presence of the carboxylic acid moiety *ortho* to the hydrazine was necessary not only for contrast production, but also for rapid hydrazone formation and prolonged hydrazone product stability under physiological conditions. This work provided the first example of an MRI-based contrast agent capable of a "turn on" response upon reaction with bioactive aldehydes, and outlined both the structural and electronic requirements to expand on Hydrazo-CEST, a novel, hydrazone-dependent subtype of diamagnetic CEST-MRI.

Introduction

Magnetic resonance imaging (MRI) is a clinical diagnostic technique employing a variety of contrast mechanisms, some of which are reliant upon the mapping of differential water proton relaxation following radiofrequency excitation in a magnetic field. MRI has traditionally been applied to anatomical and functional imaging in the clinical setting, and has been moving toward molecular-level diagnosis in part through the use of biochemical-targeted contrast agents.[1] Gadolinium-based chelates that reduce the relaxation time of neighboring water protons have previously been the focus of contrast agent development, however concerns about chelate stability in vivo has motivated a search for metal-free alternatives.[2] Chemical exchange saturation transfer (CEST) using organic (i.e., diamagnetic) probes is a recently proposed[3,4] metal-free MRI technique offering a promising alternative mode of molecular-level contrast that can overcome the toxicity concerns associated with paramagnetic agents.[5] The CEST imaging mechanism depends on a contrast agent proton that readily exchanges with water, and that possesses a sufficiently large resonance frequency offset from water ($\approx$1–3 ppm) to allow its specific spin saturation by radiofrequency irradiation (Figure 1 a). A spin saturation effectively masks the exchangeable proton from detection, reducing the post-saturation amplitude of the water peak (S) relative to its pre-saturation magnitude (S_o) (Figure 1 b). Ultimately, the suppression of water signal results in a loss of image signal (i.e., a darkening) in the immediate vicinity of the contrast agent. Since solute–water proton exchange rates (k_{sw}) for the CEST effect are typically 10^2–10^3 Hz, a few seconds of irradiation can significantly amplify the signal produced from a single contrast agent molecule.[6]

Humans are exposed to toxic aldehydes on a daily basis, both externally through the environment (e.g. acrolein, formaldehyde) and internally through highly regulated metabolic processes (e.g. acetaldehyde, 3-aminopropanal). Dysregulation of these metabolic processes, including lipid peroxidation,[7,8]

[a] *T. Dang, Dr. M. Suchy, Y. J. Truong, C. Lazurko, Dr. G. Facey, Prof. A. J. Shuhendler*
Department of Chemistry & Biomolecular Sciences
University of Ottawa
Ottawa, ON (Canada)
E-mail: adam.shuhendler@uottawa.ca

[b] *Dr. M. Suchy, Prof. A. J. Shuhendler*
University of Ottawa Heart Institute
Ottawa, ON (Canada)

[c] *Dr. W. Oakden, Dr. W. W. Lam, Prof. G. J. Stanisz*
Department of Physical Sciences
Sunnybrook Research Institute
Toronto, ON (Canada)

[d] *Prof. G. J. Stanisz*
Department of Biomedical Physics
University of Toronto
Toronto, ON (Canada)

[e] *Prof. G. J. Stanisz*
Department of Neurosurgery and Pediatric Neurosurgery
Medical University
Lublin (Poland)

Supporting information and the ORCID identification number(s) for the author(s) of this article can be found under: https://doi.org/10.1002/chem.201801671.

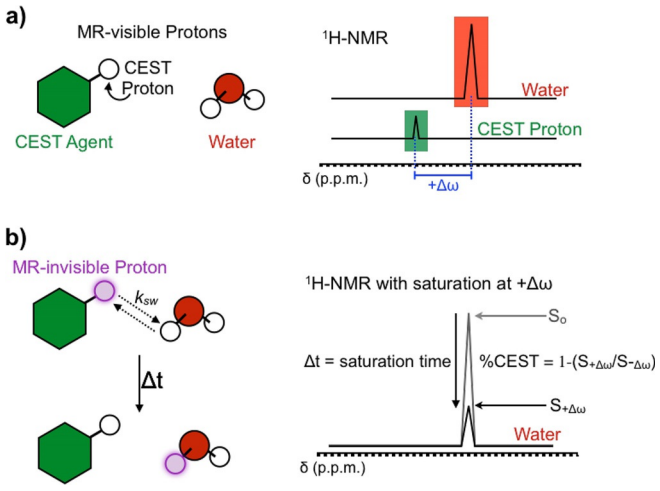

Figure 1. Chemical exchange saturation transfer (CEST) imaging works through proton exchange between contrast agent and water. (A) An exchangeable proton (white circle) on the CEST contrast agent (green hexagon) has a chemical shift that is different from that of water by ^{1}H NMR. This chemical shift difference ($+\Delta\omega$) allows the exchangeable proton on the contrast agent to be spin saturated, effectively making the exchanged water protons invisible to detection by magnetic resonance imaging (MRI). (B) The exchangeable proton on the contrast agent is spin saturated (purple circle) and undergoes exchange with water protons, effectively making water invisible to the MRI (signal peak at S_o versus that as $S_{+\Delta\omega}$). Since proton exchange occurs thousands of times per second, and since saturation is induced for approximately 3–5 seconds, thousands of water protons are "silenced" by a single contrast agent, allow the depression of water to be mapped by the MRI. The signal intensity (%CEST) is calculated as the signal ratio with and without contrast agent proton spin saturation.

carbohydrate autoxidation,[7] polyamine oxidation,[9] and myeloperoxidase activity,[7] leads to an increased production of aldehydes during chemical or mechanical stress, and throughout the course of a range of diseases. Aldehydes have been suggested to be valuable biomarkers of brain damage, ischemia-reperfusion injury, and neurodegenerative disorders,[10–12] but their detection in vivo is challenging, and has remained elusive until a very recent report by Caravan and co-workers demonstrating lung fibrosis imaging by hydroxylamine-modified gadolinium chelates.[13] This initial demonstration of the value of aldehydes as imaging biomarkers targeted allysine residues on fibrosis-associated oxidized collagen, employing a mechanism of selective probe retention in aldehyde-rich tissue environments. However, endogenous aldehydes are not usually protein-bound, but rather are small (MW $<$ 100), mobile and reactive molecules; consequently, their in vivo detection is not amenable to the "probe retention"-based imaging mechanism previously described.[13]

Within the framework of our interest in developing advanced probes for molecular imaging, we have built on the value of aldehydes as diagnostic biomarkers and designed molecular probes capable of the in vivo imaging of these small, unbound aldehydes. Two key design criteria for our probes were established: 1) the probe must react rapidly with endogenous aldehydes to form stable products; 2) a significant signal enhancement should be observed upon reaction of the molecular imaging probe with the aldehydes. To comply with both requirements, we investigated molecular probes based on the N-amino anthranilic acid (2-hydrazinobenzoic acid) scaffold. Structurally similar hydrazines have been recently shown to react with aldehydes in "click-like" fashion, with a reaction rate $> 2\,M^{-1}s^{-1}$ that is comparable to that associated with strain-promoted alkyne-azide cycloaddition.[14,15] Moreover somewhat structurally related N-substituted (*N*-phenyl, *N*-mesyl, *N*-trifluoroacetyl) anthranilic acids are known to act as diamagnetic CEST MRI contrast agents.[16] Through a detailed investigation of a small library of N-amino anthranilic acids and corresponding hydrazones, we have expanded the functionalities available for metal-free contrast agent design, demonstrated that the proton on the ring-proximal nitrogen of an aryl hydrazone is amenable to detection by CEST-MRI, and present the first CEST agent that conditionally produces signal only after binding rapidly to aldehydes under physiological conditions.

Results and Discussion

Synthetic procedures

Intermediates and final products described in this study (Figure 2) have been prepared in moderate to good yields, often times using modified literature protocols. Synthetic schemes, full experimental details and NMR spectra associated with the compounds discussed within this paper can be found in the Supporting Information.

Briefly, anthranilic acids **1a**–**1f** were diazotized ($NaNO_2$, HCl), followed by $SnCl_2{\cdot}2H_2O$-mediated reduction.[17] Corresponding hydrazines **2a**–**2f** were obtained as dihydrochlorides. Treatment of **2a**–**2f** with 2-formylbenzenesulfonic acid afforded hydrazones **3a**–**3f**; when **2a**–**2f** were treated with acetaldehyde, hydrazones **4a**–**4f** were obtained. One notable exception is hydrazone **4d**, which we were unable to isolate. To expand the library of compounds, hydrazone **2f** was treated with aldehydes or corresponding synthetic equivalents (3-aminopropanal diethyl acetal, crotonaldehyde, racemic glyceraldehyde[18] and glycolaldehyde dimer) to furnish hydrazones **5a**–**5d**. Reaction of **2f** with acetone or pyruvic acid afforded hydrazones **6a** and **6b**.

To prepare the control compounds used in this study, 5-methoxyanthranilic acid (**1f**) was esterified (Fischer esterification),[19] followed by a one pot diazotization-reduction cascade.[17] Ester hydrazine **7** was obtained as a dihydrochloride salt. Treatment of **7** with 2-formylbenzenesulfonic acid furnished hydrazone **8a**, while **8b** was prepared by reaction of **7** with acetaldehyde. Reaction of commercially available 4-methoxyphenyl hydrazine dihydrochloride (MeOPH, **9**) with 2-formylbenzenesulfonic acid led to the formation of hydrazone **10a**; despite many attempts we were unable to isolate hydrazone **10b** derived from **9** and acetaldehyde. Finally, when hydrazine **2f** was treated with malondialdehyde tetramethyl acetal,[20] pyrazole **11** was obtained. 3-Hydroxybenzoic acid (**12**) was commercially available.

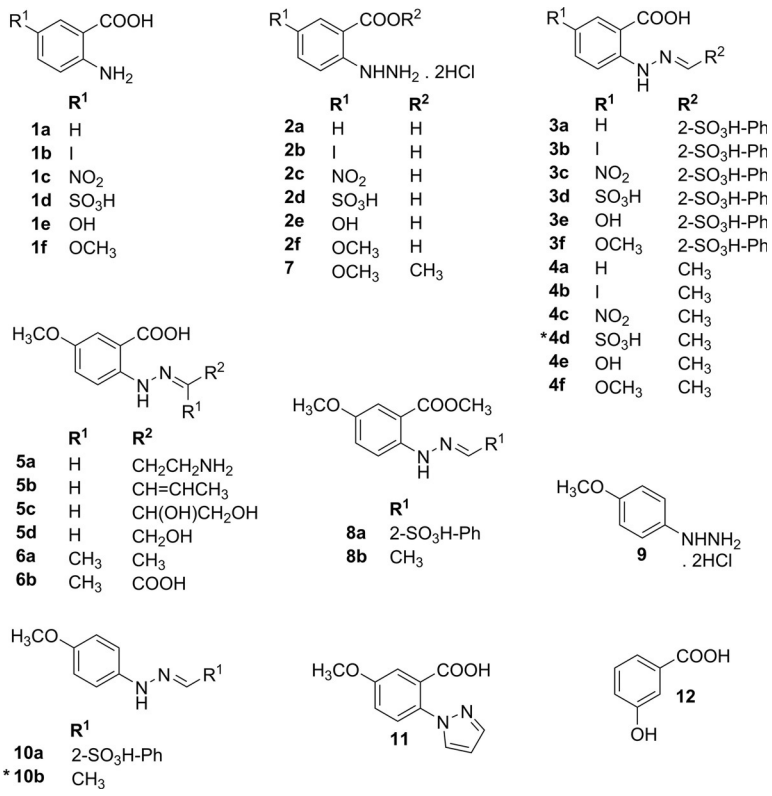

Figure 2. Chemical structure of compounds discussed in this study. * Compounds could not be isolated.

Structural requirements for CEST signal

One limitation of diamagnetic CEST contrast agents is their often-small frequency offsets (≈1–3 ppm) from water, making their signal deconvolution from the highly abundant water peak difficult.[16] Anthranilic acids have previously been identified as CEST agents with a significant 4.8–9.3 ppm CEST signal frequency offset, a result of intramolecular hydrogen bonding between the benzylic amine and a hydrogen bonding partner in the *ortho*-position.[16] We explored the effect of converting the weakly nucleophilic aromatic amine of anthranilic acid into an α-nucleophilic hydrazine with the intention of producing an aldehyde-specific imaging agent. Interestingly, the formation of the hydrazine nucleophile completely abolished proton exchange detectable by CEST methods (e.g. **2 f**), but this signal was recovered upon conversion of the probe to a hydrazone (e.g. **4 f**); only the hydrazone, but not the hydrazine, provided CEST contrast (Figure 3). To denote the set of probes behaving in a similar manner, we propose the term Hydrazo-CEST. Probe chemistries that are activated (i.e., produced detectable changes in image signals) only once bound to, or acted upon by, their intended molecular target of interest benefit from an inherent decrease of background signal, maximizing the achievable signal-to-noise ratio and imaging signal reliability. In addition, the "turn-on" mechanism of aldehyde reporting utilized by Hydra-

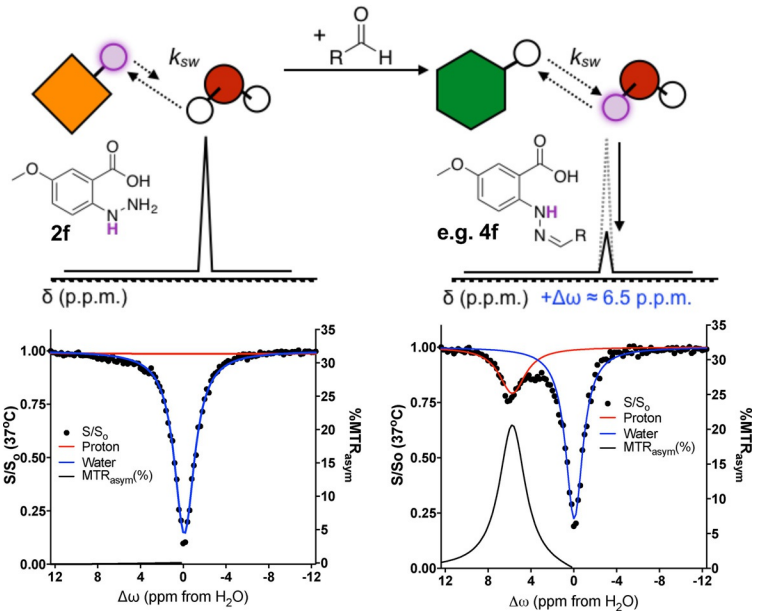

Figure 3. Hydrazo-CEST is a new mechanism of MRI contrast enhancement, with signal production selectively turned on in the presence of bioactive carbonyls (e.g. aldehydes and ketones). The exchangeable hydrazo proton (purple) does not result in the suppression of water signal when the contrast agent, based on substituted N-amino anthranilic acids, is in the hydrazine form (i.e., k_{sw} is not amenable to CEST-MRI). The rapid condensation of the hydrazine with the aldehyde or ketone to form a hydrazone results in an optimized exchange of the spin saturated proton with water, significantly reducing the water signal and producing CEST-MRI contrast enhancement (i.e., k_{sw} is ideally suited to CEST-MRI). Z-spectra were acquired at 37 °C, pH 7.4, and 40 mM concentrations. In this example, R=CH_3.

zo-CEST is independent of the anchorage of target aldehydes, and would be capable of mapping freely diffusing small molecule aldehydes as well as those derived from oxidized residues of biomacromolecules. The Hydrazo-CEST probes presented here thus take advantage of activation by endogenous aldehydes, and are an initiating class of non-optical, activatable imaging agents capable of selectively sensing endogenous reactive carbonyls.

Hydrazo-CEST probes maintain a large 6.4 ppm frequency offset, and exhibit the same requirements for a hydrogen bonding partner in the *ortho*-position as demonstrated for anthranilic acids.[16] The loss of the carboxylic acid proton through esterification results in a complete loss of the CEST effect (**8b**, Figure 4a), and the complete removal of the carboxylic acid to form a substituted phenylhydrazine (**10a**, Figure 4b) results in significant broadening and weakening of the CEST signal, and an approximate 2 ppm upfield shift. While compound **10a** exhibits some CEST signal likely due to interaction of the sulphate with the ring proximal nitrogen, the loss of the intramolecular hydrogen bonding due to removal of the *ortho* carboxylate substantially alters the CEST signal produced. The importance of this intramolecular hydrogen bond is supported through molecular modelling of aliphatic and aryl aldehyde-derived hydrazones (Figure S1). *E*/*Z* isomerization around the hydrazone bond is known,[21] which alters the relative position of the proton on the ring-proximal nitrogen, the putative exchangeable proton producing the Hydrazo-CEST signal. Density functional theory calculations using a B3LYP force field in water as solvent revealed that the *E*-isomers of both the aliphatic acetaldehyde- and aryl 2-formylbenzenesulfonic acid-derived hydrazones adopted conformations optimally positioning the ring-proximal nitrogen for intramolecular hydrogen bonding with the neighboring carboxylic acid group. The calculated geometry of the aliphatic aldehyde-derived hydrazone is that of a planar pseudo-six membered ring, with the putative exchangeable proton bonding directly with the carboxyl oxygen. The aryl aldehyde-derived hydrazone formed a more strained pseudo-six membered ring, with the ring-proximal nitrogen hydrogen bonding to the carboxyl proton (Figure S1). ^{1}H NMR spectra of the acetaldehyde-derived hydrazone (**4f**) show both *E*- and *Z*-isomers, with *E* predominating 2:1 over the *Z*-isomer, and the *cis* conformation of the hydrazone bond predominating 2:1 over the *trans* conformation. Only the *E*-isomer is observed in the ^{1}H NMR of the 2-formylbenzenesulfonic acid-derived hydrazone (**3f**), which is in agreement with our molecular modelling that was unable to minimize the energy associated with the *Z*-isomer for this structure (Figure S1).

The characterization of the structural requirements for Hydrazo-CEST continued by the removal of the α-nucleophile but retention of the carboxylic acid, which nearly completely abolished Hydrazo-CEST signal production (Figure 4c). Finally, we sought to confirm that the proton on the ring-proximal nitrogen was actually the proton exchanging with water to induce the Hydrazo-CEST effect. Complete abolishment of signal production was observed with pyrazole **11** possessing no exchangeable proton on the ring proximal nitrogen (Figure 4d), supporting the hypothesis that indeed the proton on the ring-proximal nitrogen is the exchangeable proton giving rise to

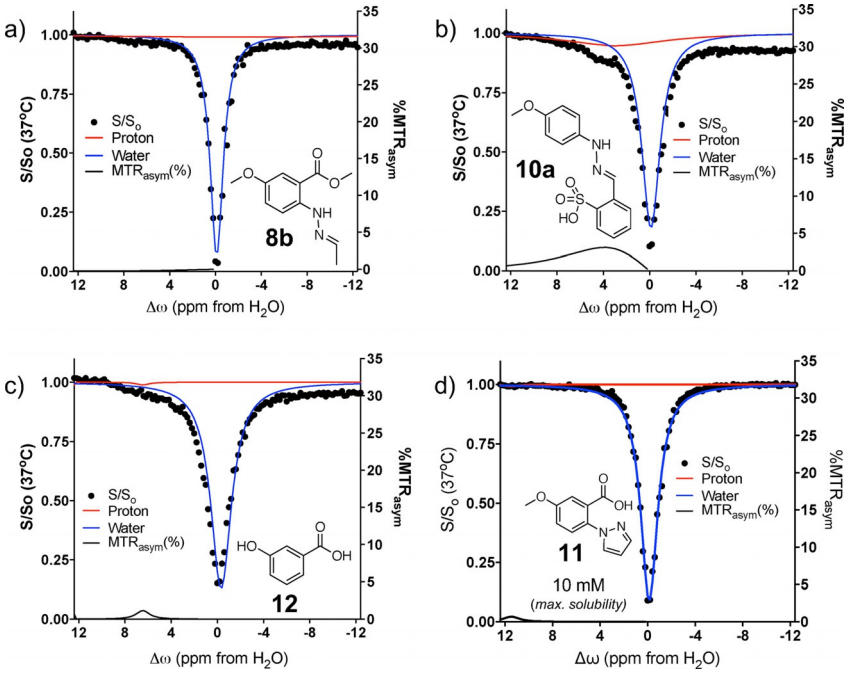

Figure 4. Z-spectra demonstrating the requirements of both the hydrazone and *o*-carboxylic acid for the production of contrast for CEST-MRI. The masking of the *o*-carboxylic acid as the methyl ester (a) or its complete absence (b) significantly impairs CEST-MRI signal generation. Likewise the absence of the hydrazine moiety nearly completely abolishes signal production (c). The absence of the hydrazone proton through the formation of a pyrazole also completely abolishes CEST-MRI signal (d). Raw data points (S/S_o, black circles), exchangeable proton (red) and water (blue) Lorentzian curves, and CEST-MRI signal production (MTR_{asym}(%), black curve) are shown. All Z-spectra are obtained at 37 °C and pH 7.4 with 40 mM compound solutions in 10:1 PBS:D_2O unless otherwise indicated.

Hydrazo-CEST. Therefore, both computational and experimental data highlight the importance of the conformation of the hydrazone bond to position the exchangeable hydrogen, which is indeed that on the ring-proximal nitrogen, for hydrogen bonding with the necessary carboxylic acid group in the *ortho* position.

Kinetics of hydrazone formation and stability studies

To take advantage of the enhanced signal-to-noise ratio provided by the aldehyde-dependent activation of Hydrazo-CEST, the formation of the hydrazone from N-amino anthranilic acid must occur in situ under physiological conditions. The rates of reaction of carbonyls with hydrazine-derived nucleophiles have previously been well-characterized.[14,15] It was found that intramolecular acid/base catalysis significantly enhanced the rate of hydrazone formation, with the reaction of butanal and 2-hydrazinobenzoic acid (**2 a**) having a *pseudo*-first-order rate constant (k_{obs}) of $1.5 \pm 0.2\ min^{-1}$ in a 1:10 DMF: PBS solution. Repeating the methodology outlined previously,[14] however at 37 °C in 100% 1× PBS, we determined the k_{obs} for the reaction of 5-methoxy N-amino anthranilic acid (**2 f**) and related analogues with 2-formylbenzenesulfonic acid (Figure 5, Supporting Information Figure S2) and acetone (Figure S3). The calculated k_{obs} are summarized in Table S1. Under the conditions employed, the k_{obs} for hydrazone formation from **2 f** with 2-formylbenzenesulfonic acid was an order of magnitude faster than with acetone. This difference in reaction rate was previously observed among carbonyl compounds, with hydrazone formation from aldehydes proceeding faster than from ketones.[14,15] Likewise, the k_{obs} for hydrazone formation from 2-formylbenzenesulfonic acid and **7**, a methyl ester analogue of **2 f**, was slowed by three orders of magnitude, which was previously observed and attributed to the increased bulk of the methyl ester relative to the carboxylic acid.[14] Importantly, substantial differences were observed in the extent of reaction completion and product stability, in addition to rate of reaction, between hydrazine structures for a given aldehyde, as well as between carbonyl types for a given hydrazine (Table S1).

Hydrazone stability was assayed both spectrophotometrically (Figure 5 a, S2 a vs. b), as well as by HPLC (Figure 5 b). While the formation of hydrazone from **2 f** and 2-formylbenzenesulfonic acid reached ≈90% completion within 30 min of initiation (Figure 5 a, black curve), the absence of the intramolecular acid/base catalyst, as in the reaction of 4-methoxyphenylhydrazine (**9**) or **7** with the same aryl aldehyde, substantially reduced reaction completion (<25% maximum; Figure 5 a, red and blue curves, respectively), and reduced stability of the hydrazone product (Figure 5 b). This data suggests a role for the *ortho*-carboxylic acid in product stabilization, in addition to the catalytic effect previously observed.[14] A similar difference in reaction completion was observed for the reaction of **2 f** with acetone, resulting in <25% product formation (Figure S3). Under the buffer and temperature conditions studied (i.e., 37 °C and 1×PBS), the rate of the reaction, the extent of reaction completion, and the stability of the hydrazone product

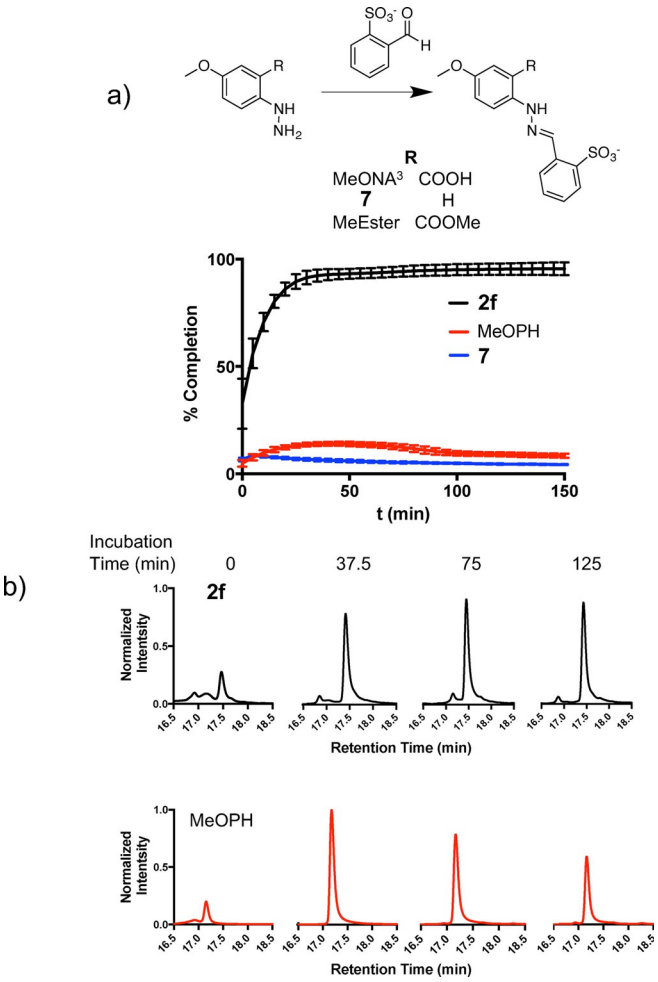

Figure 5. The *o*-carboxylic acid contributes to substantial reaction completion as well as extended stability of the product hydrazone under physiological conditions. (a) Kinetic plots for the reaction of N-amino anthranilic acid (**2 f**), MeOPH (red), or the methyl ester of **2 f** (compound **7**) (blue) with 2-formylbenzenesulfonic acid are shown, demonstrating that the carboxylic acid moiety is necessary for driving the reaction to completion, and to maintaining the stability of the hydrazone product. (b) High-pressure liquid chromatography traces of the reaction of **2 f** (black) and MeOPH (red) with 2-formylbenzenesulfonic acid. The hydrazone peak is shown (r.t. = 17.5 min for **2 f** and 17.2 min for MeOPH) at the time points indicated. All reactions were performed in 1× PBS at 37 °C, and points represent mean ± s.d. for $n = 3$ trials.

were all substantially improved in the presence of the *ortho*-carboxylic acid. Since the signal produced by Hydrazo-CEST depends on the hydrazone form of the probe, the faster-forming and longer-lived the hydrazone product under physiological conditions, the better the imaging signal evolved and the more potentially sensitive the imaging technique.

Electronic requirements for CEST signals

After demonstrating the structural requirement of the *ortho*-carboxylic acid moiety for Hydrazo-CEST signal production and the rapid, stable, and aldehyde-preferential formation of hydrazone under physiological conditions, the electronic contributions to Hydrazo-CEST were evaluated. Electron donating (OH,

OCH_3) and electron-withdrawing (I, SO_3, NO_2) substituents were appended at the 5-position of N-amino anthranilic acid (compounds **2b–f**), both acetaldehyde (**4b–f**) or 2-formylbenzenesulfonic acid-derived hydrazones (**3b–f**) were prepared, and Z-spectra were acquired in 1:10 D_2O:PBS at pH 7.4 on a 300 MHz NMR (Figures S4–5).

Hydrazo-CEST signal production (%MTR_{asym}) was normalized to hydrazone concentration, as different hydrazone species showed different maximum solubility in neutral buffer (Figure S6–7). In this way, per molar signal output could be compared across hydrazone series to examine electronic contributions to Hydrazo-CEST (Figure 6). Importantly, Hydrazo-CEST as a contrast mechanism produced as much signal as the aspirin metabolite salicylate (Figure 6, grey bar), a diamagnetic CEST agent recently shown to have very high signal production.[22,23] Ring deactivating substituents at the 5-position on the N-amino anthranilic acid substantially reduced Hydrazo-CEST signal relative to the unsubstituted parent compound. For the acetaldehyde-derived hydrazones **4a–4f**, a decrease in Hydrazo-CEST signal relative to the unsubstituted parent hydrazone was observed with an increasing strength of ring activation. However, the 2-formylbenzenesulfonic acid-derived hydrazones **3a–3f** showed the opposite effect: an increase in Hydrazo-CEST signal production with an increase in ring activation potential.

In efforts to explain these trends in signal production, the rate of exchange between bulk water and the proton on the ring-proximal nitrogen, k_{sw}, were measured by varying the saturation pulse power, as previously described,[24] and the values are shown in Figure 6. Indeed, the change in %MTR_{asym} induced by altering the electronics through the 5-position of the hydrazine ring paralleled the change in k_{sw}. The importance of the contribution of the aryl hydrazine electronics to signal generation is supported by the linear free energy relationship between the chemical shift of the exchangeable hydrazone proton and the normalized proton exchange rates ($R^2 = 0.990$) (Figure S8). Additionally, the aldehyde binding partner contributes to k_{sw} of the proton on the ring-proximal nitrogen, likely via the π-conjugation maintained through the hydrazone bond (Figure S9). The *o*-sulfo substituent of the aryl aldehyde is more electron-withdrawing than the aliphatic carbon of the acetaldehyde, reducing electron density around the hydrazone bond (e.g. **3f** versus **4f**). While the exchange process of this system is complicated by the intramolecular hydrogen bond provided by the *ortho* carboxylate, overall the data suggests that electronic contributions of both the aldehyde and hydrazine binding partners affect per molar normalized imaging signal by modulating the exchange rate of the proton on the ring-proximal nitrogen with water.

Concentration- and pH-dependence of Hydrazo-CEST signal

The MRI contrast produced by CEST probes is dependent upon voxel-wise concentration, however previous investigations have reported non-linear concentration relationships for CEST contrast agents.[25] In order to evaluate this dependence for Hydrazo-CEST compounds, Z-spectra were acquired for acetaldehyde (**4b–4f**) and 2-formylbenzenesulfonic acid-derived hydrazones (**3b–3f**) on a 300 MHz NMR from 5 mM to 40 mM, or the maximum solubility of the compound in neutral buffer (Figure S6–7). The dynamic range for Hydrazo-CEST signal production from each compound was then plotted using the maximum signal for each compound (6.4 ± 0.4 ppm). Within the series of acetaldehyde-derived hydrazones, the 5-methoxy- (**4f**) and 5-hydroxy-substituted (**4e**) analogues had the broadest dynamic range for imaging signal (Figure S10a, green and blue curves, respectively), with the 5-methoxy-derivative showing the higher absolute %MTR_{asym} and the most linear concentration-dependent signal production ($R^2 = 0.98$). While the signal production at 20 mM was highest for the unsubstituted hydrazone (**4a**) relative to **4e** and **4f**, its low sensitivity to changes in concentration below 10 mM and limited solubility beyond 20 mM substantially narrowed its dynamic range. For the series of 2-formylbenzenesulfonic acid-derived hydrazones, the 5-hydroxy-substituted (**3e**) analogue displayed the best dynamic range with the most linear concentration-dependent signal production ($R^2 = 0.98$) of all of the analogues examined (Figure S10b, blue curve). In fact, both the unsubstituted (**3a**) and 5-methoxy-substituted (**3f**) analogues displayed non-linear concentration dependence over the range of concentrations examined (Figure S10b, red and green curves, respectively). Importantly, the signal production from **4f** at 5 mM

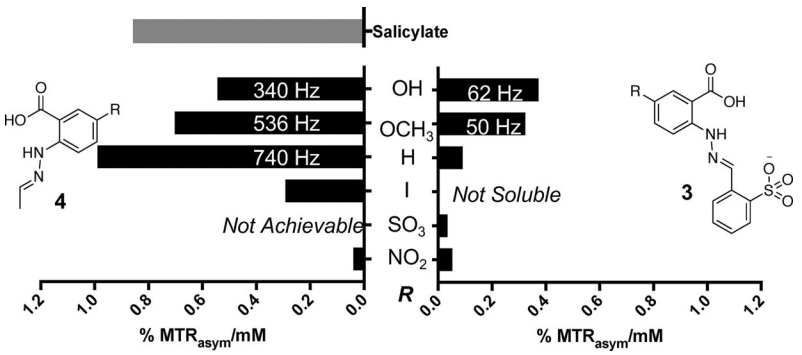

Figure 6. The substitution of both the hydrazine and carbonyl substantially impact the CEST-MRI signal generation from Hydrazo-CEST contrast agents. The concentration-normalized Hydrazo-CEST signal (%MTR_{asym}/mM, black bars) is plotted for hydrazones formed by different substituents at the 5-position of the aryl hydrazine moiety, and with aliphatic (**4**) or aromatic (**3**) aldehydes. Signal production can be directly compared to salicylate, a known diamagnetic CEST agent (grey). Note: Sulfo-substituted hydrazine did not form a hydrazone with acetaldehyde. Values shown on plot are k_{sw} in Hz.

(MTR_{asym} = 9%) has been shown to be suitable for detection in vivo by CEST-MRI,[16,26] and is on par on a per molar basis with salicylate, a diamagnetic CEST-MRI contrast agent readily detectable in vivo.[23]

In addition to local probe concentrations, microenvironmental pH can modify CEST signal production, as pH directly impacts k_{sw}.[4,27] The effect of pH on $\%MTR_{asym}$ was evaluated for the unsubstituted, 5-hydroxy-, and 5-methoxy-substituted hydrazones derived from acetaldehyde (**4a, 4e, 4f**) and 2-formylbenzenesulfonic acid (**3a, 3e, 3f**) (Figure S11). The aliphatic aldehyde-derived hydrazones displayed a broad pH range (approx. pH 6 to 8) over which high CEST signal production was observed, with maximum signal occurring between pH 6.5 and 7.5. The 5-methoxy-substituted probe (**4f**) produced significantly higher CEST signal at all pH values tested. Note that **4f** was not soluble at 40 mM at pH 6.5, however both **4a** and **4e** were completely soluble from pH 6.0–8.0. In contrast, the $\%MTR_{asym}$ from aromatic aldehyde-derived hydrazones was substantially reduced above pH 6.5–7.0, with maximum signal generation occurring below pH 6.5. The hydroxy- and methoxy-substituted aryl-hydrazones (**3e**, **3f**) gave better CEST signal production from pH 6.5–8.0, but both were insoluble at 40 mM at pH 6.0. The differential pH responses associated with the HydrazoCEST probes studied are justified by the higher predicted electron density around the ring-proximal nitrogen of the aliphatic versus aromatic hydrazones (Figure S9), which would favor the protonated form of the hydrazo moiety at higher pH values. Since the majority of endogenously formed aldehydes are non-aromatic,[7] the 5-methoxy-substituted analogue (**2f**) was selected as the lead compound for endogenous aldehyde detection with Hydrazo-CEST due to its superior dynamic range with aliphatic aldehydes and enhanced signal generation at neutral pH.

Detection of endogenous carbonyls

Having optimized Hydrazo-CEST probe chemistry for high signal production in physiological conditions, signal generation from endogenous carbonyls was explored. Z-spectra were generated for a variety of hydrazones formed from **2f** and endogenous aldehydes and ketones (Figure 7): **5a** is the hydrazone of 3-aminopropanal, a product of polyamine catabolism suggested to be elevated following traumatic brain injury (Figure 7a);[11,12] **5b** is the hydrazone product of crotonaldehyde, a terminal product of lipid peroxide catabolism following cell stress (Figure 7b);[7] **5c** is the hydrazone formed from glyceraldehyde, the glycolytic intermediate required for phospholipid biogenesis (Figure 7c); **6b** is the hydrazone product of **2f** and pyruvate, a key biochemical intermediate for a variety of biosynthetic and metabolic pathways including anaerobic glycolysis (Figure 7d). Importantly, there was no hydrazone formation between **2f** and D-glucose under physiological conditions (37 °C, 1×PBS, pH 7.4) within 4 h of incubation, suggesting glucose will not interfere with aldehyde sensing by Hydrazo-CEST.

Hydrazo-CEST MRI

As further support of this novel class of contrast agent for aldehyde-activated imaging, we validated the performance of Hydrazo-CEST by 3 T and 7 T MRI (Figure 8). Just as observed in the NMR, the hydrazine form of the probe (**2f**) produced no CEST contrast (Figure 8a, left), however signal production was

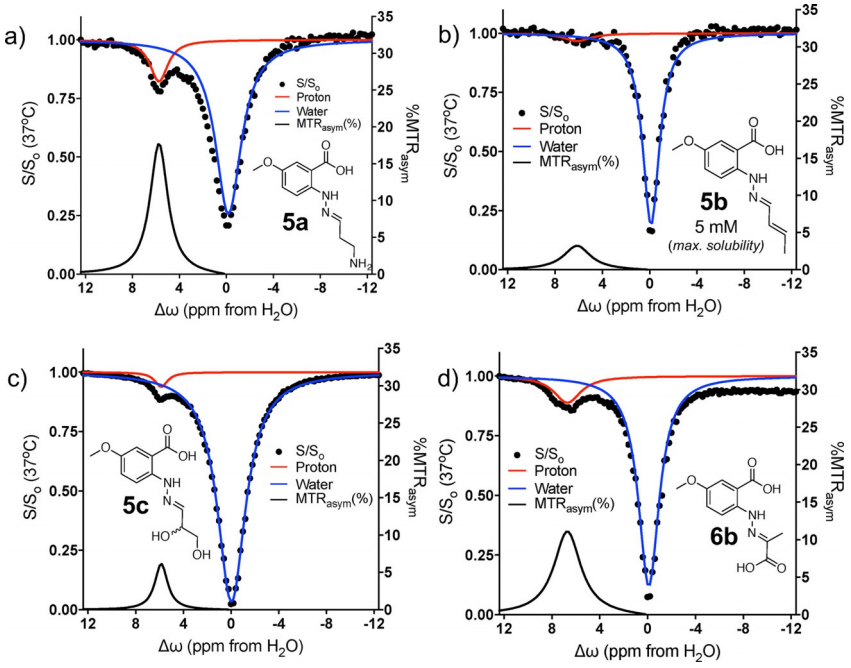

Figure 7. Hydrazo-CEST signal production from endogenous carbonyls. Z-spectra were acquired on a 300 MHz NMR in 10:1 PBS:D_2O at 37 °C, pH 7.4, at 40 mM, or the indicated concentration providing maximum solubility. Hydrazones were formed between **2f** and a) 3-aminopropanal, b) crotonaldehyde, c) glyceraldehyde, and d) pyruvate.

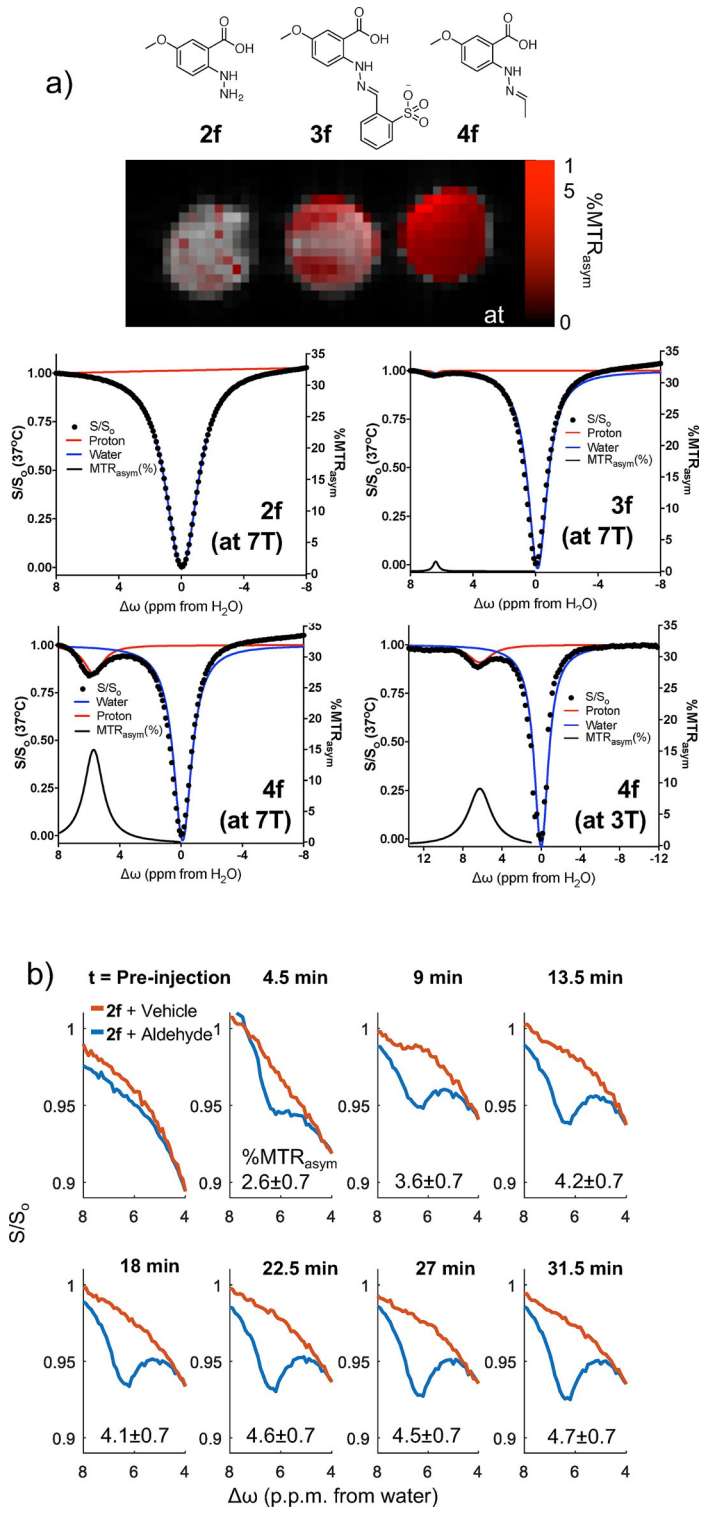

Figure 8. Hydrazo-CEST probes provide high contrast and rapidly form hydrazones in situ. a) Phantom image and Z-spectra of hydrazine **2 f** and hydrazones **3 f** and **4 f** were acquired at the indicated field strength, 37 °C, pH 7.4, and 40 mM concentration. b) Z-spectra were acquired following the addition of vehicle (red) or 2-FB (blue) to a 40 mM solution of hydrazine **2 f** at 37 °C and pH 7.4. Values indicate the $\%MTR_{asym} \pm$ the standard deviation of the off-resonance measurements once the system had reached steady state.

substantially increased following hydrazone formation from either aliphatic (**4 f**) or aromatic aldehydes (**3 f**) with a frequency offset from water of 6.4 ppm. The kinetics of Hydrazo-CEST signal production through hydrazone formation were also evaluated in the MRI at 37 °C in 1×PBS at pH 7.4 (Figure 8 b). Either PBS (red curve) or a PBS solution of 2-formylbenzenesulfonic acid at a final concentration of 20 mM (blue curve) were injected into the imaging phantom, and Z-spectra were acquired every 4.5 min to monitor hydrazone formation. A single saturation peak at 6.4 ppm was observed 4.5 min after aldehyde injection. The Hydrazo-CEST signal increased rapidly, surpassing 50% maximal signal within the first 4.5 min, and reaching a maximum plateau ($\%MTR_{asym}$ 4.6 ± 0.7) by 18 to 22.5 minutes after aldehyde addition. This MRI data confirms that Hydrazo-CEST probes are rapidly activated by aldehydes under physiological conditions, and are readily detectable by 3 T and 7 T MRI. Both hydrazine and hydrazone functionalities are utilized in medications broadly spanning indications from anti-infectives and anti-parasitics, to anti-cancer agents.[28] Taken together with preliminary in vitro toxicity assays demonstrating the initial safety of **2 f** (Figure S12), the substantial signal production (approx. 20% MTR_{asym}) by the 3-aminopropanal-derived hydrazone (**5 a**), the limited signal production by metabolic aldehyde (glyceraldehyde, **5 c**), and the limited hydrazone formation rates between **2 f** and ketones, such as pyruvate (**6 b**) (Figure S3) supports that Hydrazo-CEST is potentially valuable as a first-in-class, aldehyde-activated MRI contrast agent for mapping these endogenous markers of tissue stress.

Conclusion

In conclusion, we have developed a new class of CEST-MRI contrast agents derived from N-amino anthranilic acids, termed Hydrazo-CEST, which conditionally respond to the presence of some endogenous aldehydes upon in situ transformation from hydrazine to hydrazone. The "turn-on" mechanism of aldehyde reporting utilized by Hydrazo-CEST is independent of the anchorage of target aldehydes, and would be capable of mapping freely diffusing small molecule aldehydes as well as those derived from oxidized residues of biomacromolecules. The importance of the carboxylic acid *ortho* to the α-nucleophile was investigated, demonstrating its absolute requirement for signal production, as well as for rapid hydrazone formation and extended product stability under physiological conditions. Additionally, the electronic requirements providing optimal CEST contrast have been identified, with electron-donating substituents at the 5-position (i.e., hydroxy and methoxy) providing superior performance in terms of signal generation over the ranges of concentrations and pH expected in living subjects. The rapid reaction with aldehydes and high CEST MRI signal production at 3 T and 7 T support the application of these probes for the detec-

tion and mapping of endogenous aldehydes in living subjects. With Hydrazo-CEST, small molecule, endogenous aldehyde biomarkers of disease may now be accessible to mapping, allowing chemical biological investigations of these important biomolecules.

Supporting Information

Supporting Information is available from the Wiley Online Library or from the author.

Acknowledgements

This work was supported by an NSERC Discovery Grant RGPIN 2015-05796 (A.J.S.), the Canada Research Chairs Program 950-230754 (A.J.S.), the Canadian Foundation for Innovation (A.J.S.), and the Canadian Institutes of Health Research PJT376892 (A.J.S.).

Conflict of interest

The authors declare no conflict of interest.

Keywords: aldehydes · chemical exchange saturation transfer · contrast agents · hydrazones · magnetic resonance imaging

[1] a) M. Haris, S. K. Yadav, A. Rizwan, A. Singh, E. Wang, H. Hariharan, R. Reddy, F. M. Marincola, *J. Transl. Med.* **2015**, *13*, 313; b) A. J. Shuhendler, D. Ye, K. D. Brewer, M. Bazalova-Carter, K. H. Lee, P. Kempen, K. Dane Wittrup, E. E. Graves, B. Rutt, J. Rao, *Sci. Rep.* **2015**, *5*, 14759.

[2] a) R. J. McDonald, J. S. McDonald, D. F. Kallmes, M. E. Jentoft, M. A. Paolini, D. L. Murray, E. E. Williamson, L. J. Eckel, *Radiology* **2017**, *285*, 546 – 554; b) T. Kanda, H. Oba, K. Toyoda, K. Kitajima, S. Furui, *J. Radiol.* **2016**, *34*, 3; c) R. J. McDonald, J. S. McDonald, D. F. Kallmes, M. E. Jentoft, D. L. Murray, K. R. Thielen, E. E. Williamson, L. J. Eckel, *Radiology* **2015**, *275*, 772; d) A. Rajca, Y. Wang, M. Boska, J. T. Paletta, A. Olankitwanit, M. A. Swanson, D. G. Mitchell, S. S. Eaton, G. R. Eaton, S. Rajca, *J. Am. Chem. Soc.* **2012**, *134*, 15724.

[3] A. Bar-Shir, J. W. Bulte, A. A. Gilad, *ACS Chem. Biol.* **2015**, *10*, 1160.

[4] K. M. Ward, R. S. Balaban, *Magn. Reson. Med.* **2000**, *44*, 799.

[5] A. D. Sherry, P. Caravan, R. E. Lenkinski, *J. Magn. Reson. Imaging* **2009**, *30*, 1240.

[6] a) G. Liu, X. Song, K. W. Chan, M. T. McMahon, *NMR Biomed.* **2013**, *26*, 810; b) P. C. M. van Zijl, W. W. Lam, J. Xu, L. Knutsson, G. J. Stanisz, *NeuroImage* **2018**, *168*, 222 – 241.

[7] P. J. O'Brien, A. G. Siraki, N. Shangari, *Crit. Rev. Toxicol.* **2005**, *35*, 609.

[8] Z. A. Zielinski, D. A. Pratt, *J. Org. Chem.* **2017**, *82*, 2817.

[9] R. A. Casero, A. E. Pegg, *Biochem. J.* **2009**, *421*, 323.

[10] a) D. G. Anderson, V. R. Florang, J. H. Schamp, G. R. Buettner, J. A. Doorn, *Chem. Res. Toxicol.* **2016**, *29*, 1098; F. Di Domenico, A. Tramutola, D. A. Butterfield, *Free Radical Biol. Med.* **2017**, *111*, 253; b) A. Halstrom, E. MacDonald, C. Neil, G. Arendts, D. Fatovich, M. Fitzgerald, *J. Clin. Neurosci.* **2017**, *35*, 104; c) H. C. Wang, Y. J. Lin, F. Y. Shih, H. W. Chang, Y. J. Su, B. C. Cheng, C. M. Su, N. W. Tsai, Y. T. Chang, A. L. Kwan, C. H. Lu, *World Neurosurg.* **2016**, *87*, 463; d) L. Lorente, M. M. Martín, P. Abreu-González, L. Ramos, M. Argueso, J. J. Cáceres, J. Solé-Violán, J. M. Lorenzo, I. Molina, A. Jiménez, *J Neurotrauma* **2015**, *32*, 1; e) P. L. Wood, M. A. Khan, J. R. Moskal, *Brain Res.* **2007**, *1145*, 150.

[11] P. L. Wood, M. A. Khan, J. R. Moskal, K. G. Todd, V. A. Tanay, G. Baker, *Brain Res.* **2006**, *1122*, 184.

[12] S. Ivanova, G. I. Botchkina, Y. Al-Abed, M. Meistrell, F. Batliwalla, J. M. Dubinsky, C. Iadecola, H. Wang, P. K. Gregersen, J. W. Eaton, K. J. Tracey, *J. Exp. Med.* **1998**, *188*, 327.

[13] a) H. H. Chen, P. A. Waghorn, L. Wei, L. F. Tapias, D. T. Schuhle, N. J. Rotile, C. M. Jones, R. J. Looby, G. Zhao, J. M. Elliott, C. K. Probst, M. Mino-Kenudson, G. Y. Lauwers, A. M. Tager, K. K. Tanabe, M. Lanuti, B. C. Fuchs, P. Caravan, *JCI Insight* **2017**, *2*, e91506; b) P. Désogère, L. F. Tapias, T. A. Rietz, N. Rotile, F. Blasi, H. Day, J. Elliot, B. C. Fuchs, M. Lanuti, P. Caravan, *J. Nucl. Med.* **2017**, *58*, 1991; c) P. A. Waghorn, C. M. Jones, N. J. Rotile, S. K. Koerner, D. S. Ferreira, H. H. Chen, C. K. Probst, A. M. Tager, P. Caravan, *Angew. Chem. Int. Ed.* **2017**, *56*, 9825; *Angew. Chem.* **2017**, *129*, 9957.

[14] E. T. Kool, D. H. Park, P. Crisalli, *J. Am. Chem. Soc.* **2013**, *135*, 17663.

[15] E. T. Kool, P. Crisalli, K. M. Chan, *Org. Lett.* **2014**, *16*, 1454.

[16] X. Song, X. Yang, S. Ray Banerjee, M. G. Pomper, M. T. McMahon, *Contrast Med. Mol. Imaging* **2015**, *10*, 74.

[17] D. Kovács, J. Molnár-Tóth, G. Blaskó, I. Fejes, M. Nyerges, *Synth. Commun.* **2015**, *45*, 1675.

[18] H. Zellner, *Monatsh. Chem.* **1949**, *80*, 330.

[19] C. Theeraladanon, M. Arisawa, A. Nishida, M. Nakagawa, *Tetrahedron* **2004**, *60*, 3017.

[20] M. B. Young, J. C. Barrow, K. L. Glass, G. F. Lundell, C. L. Newton, J. M. Pellicore, K. E. Rittle, H. G. Selnick, K. J. Stauffer, J. P. Vacca, P. D. Williams, D. Bohn, F. C. Clayton, J. J. Cook, J. A. Krueger, L. C. Kuo, S. D. Lewis, B. J. Lucas, D. R. McMasters, C. Miller-Stein, B. L. Pietrak, A. A. Wallace, R. B. White, B. Wong, Y. Yan, P. G. Nantermet, *J. Med. Chem.* **2004**, *47*, 2995.

[21] S. M. Landge, E. Tkatchouk, D. Benítez, D. A. Lanfranchi, M. Elhabiri, W. A. Goddard, I. Aprahamian, *J. Am. Chem. Soc.* **2011**, *133*, 9812.

[22] a) G. Fernández-Cuervo, K. A. Tucker, S. W. Malm, K. M. Jones, M. D. Pagel, *Bioconjugate Chem.* **2016**, *27*, 2549 – 2557; b) I. Daryaei, M. M. Ghaffari, K. M. Jones, M. D. Pagel, *ACS Sens.* **2016**, *1*, 857.

[23] X. Song, P. Walczak, X. He, X. Yang, M. Pearl, J. W. Bulte, M. G. Pomper, M. T. McMahon, M. Janowski, *J. Cereb. Blood Flow Metab.* **2016**, *36*, 1186.

[24] W. T. Dixon, J. Ren, A. J. Lubag, J. Ratnakar, E. Vinogradov, I. Hancu, R. E. Lenkinski, A. D. Sherry, *Magn. Reson. Med.* **2010**, *63*, 625.

[25] D. V. Hingorani, L. A. Montano, E. A. Randtke, Y. S. Lee, J. Cárdenas-Rodríguez, M. D. Pagel, *Contrast Med. Mol. Imaging* **2016**, *11*, 130.

[26] a) S. Sinharay, E. A. Randtke, K. M. Jones, C. M. Howison, S. K. Chambers, H. Kobayashi, M. D. Pagel, *Magn. Reson. Med.* **2017**, *77*, 2005; b) L. Zhang, A. F. Martins, Y. Mai, P. Zhao, A. M. Funk, M. V. Clavijo Jordan, S. Zhang, W. Chen, Y. Wu, A. D. Sherry, *Chemistry* **2017**, *23*, 1752.

[27] S. Aime, A. Barge, D. Delli Castelli, F. Fedeli, A. Mortillaro, F. U. Nielsen, E. Terreno, *Magn. Reson. Med.* **2002**, *47*, 639.

[28] a) G. Verma, A. Marella, M. Shaquiquzzaman, M. Akhtar, M. R. Ali, M. M. Alam, *J. Pharm. Bioallied Sci.* **2014**, *6*, 69; b) R. Narang, B. Narasimhan, S. Sharma, *Curr. Med. Chem.* **2012**, *19*, 569; c) Ł. Popiołek, *Med. Chem. Res.* **2017**, *26*, 287.

Manuscript received: April 4, 2018
Accepted manuscript online: April 12, 2018
Version of record online: June 6, 2018